

# High resolution observations of the ocean upper layer south of Cape São Vicente, western northern margin of the Gulf of Cadiz.

*Sarah A. Rautenbach<sup>3</sup>, Carlos Mendes de Sousa<sup>1,2</sup>, Mafalda Carapuço<sup>4</sup>, Paulo Relvas<sup>1</sup>*

*1 Centre of Marine Sciences (CCMAR), University of Algarve, Faro, Portugal*

*2 Portuguese Institute for the Sea and Atmosphere (IPMA, I.P.), Lisboa, Portugal*

*3 Deltares, Delft, The Netherlands*

*4 Atlantic International Research Centre, Azores, Portugal*

## Abstract

This article presents an Eulerian physical and biogeochemical data set from the Iberian Margin Cape São Vicente Ocean Observatory (IbMa-CSV), a facility of the European Multidisciplinary Seafloor and water column Observatory - European Research Infrastructure Consortium (EMSO-ERIC) located 10 nautical miles south of Cape São Vicente (Portugal), the southwest tip of the Iberian Peninsula and western limit of the northern margin of the Gulf of Cadiz. The observatory was installed on the shelf break, and the data time series spans four months for most of the variables. The upper 150 m were sampled intensively with a wave powered vertical profiler at an average rate of 4.5 profiles per hour recording at 2 Hz when ascending at approximate velocity of 0.2 m/s and 10 Hz when descending at variable velocity. The vertical resolution was always higher than 0.2 m. Measured channels were conductivity, temperature, pressure, chlorophyll *a*, dissolved O<sub>2</sub> concentration, and turbidity. Derived channels are sea pressure, depth, salinity, speed of sound, specific conductivity, dissolved O<sub>2</sub> saturation, density anomaly, spiciness and Brunt-Väisälä frequency. The acquired data set includes the flow velocity and direction along the water column, taken from an upward looking 300 kHz Acoustic Doppler Current Profiler (ADCP) recorded every hour for 3 m depth bins extending the same depth range of the vertical profiler. A standard quality control scheme was applied to the data set. The data set is preserved for multiple use and is accessible in the Sea Open Scientific Data Publication (SEANOE) repository, under the address: <https://www.seanoe.org/data/00836/94769/> (Rautenbach et al., 2022).

**Key words:** High resolution dataset, vertical profiles, EMSO-ERIC, IbMa-CSV observatory, Cape São Vicente, Western Gulf of Cadiz

## 32 **1. Introduction: the relevance of the site's location**

33 The Iberian Peninsula (Figure 1) represents the northern branch of the Canary Current Upwelling System  
34 (CCUS), one of the four Eastern Boundary Upwelling Systems (EBUS), along with the Benguela,  
35 California and Humboldt or Peru upwelling systems. These systems are characterized by the coastal  
36 upwelling of cold nutrient rich subsurface water, driven by the joint action of northerly winds that blow  
37 at least during a substantial part of the year, and the Earth's rotation (Ekman mechanism). Therefore,  
38 those systems are among the most productive of the world ocean, which justifies their socio-economic  
39 relevance.

40 The CCUS is unique among the EBUS, since it is the only one punctuated by a discontinuity that is  
41 imposed by the entrance of the Mediterranean Sea into the Gulf of Cadiz (GoC) through the Strait of  
42 Gibraltar (Figure 1). The meridional coast of the western Iberian Peninsula is abruptly interrupted at the  
43 Cape São Vicente (CSV), the southwestern tip of the Iberian Peninsula. There, the coastline turns almost  
44 at a right angle into the zonal orientated northern margin of the GoC.

45 The continental shelf off the southern part of the western Iberia and in the CSV area is narrow (< 10 km  
46 wide south of 38° N), approximately delimited by the 200 m bathymetric contour. Over the continental  
47 shelf and slope, roughly from April to October, the oceanographic conditions are largely dominated by  
48 the upwelling process and associated cold jet flowing equatorward (Relvas and Barton, 2002). For the  
49 remainder of the year, the flow is expected to point northward, although there is a lack of observational  
50 evidence. Nevertheless, there is measured evidence that over the inner shelf the upwelling pattern is  
51 interrupted by the development of a warm coastal counter-current whenever the upwelling favorable  
52 winds relax below a certain threshold (Relvas and Barton 2005; Garel et al., 2016).

53 The Coastal Transition Zone, defined as the region where the coastal waters interact with the offshore  
54 oceanic waters, is populated by a variety of mesoscale structures, such as meanders, eddies, and  
55 filaments. The CSV is the root of a recurrent upwelling filament that may extend more than 150 km  
56 offshore (Sanchez et al., 2008), exporting to the open ocean a much larger mass than expected by the  
57 purely wind-driven Ekman circulation. The new production of an upwelling season could be entirely  
58 exported to the open ocean by upwelling filaments (Aristegui et al., 2006), revealing the importance of  
59 such features to the ecosystem functioning.

60 At deeper levels, where the wind is not a forcing factor, the CSV region reveals fascinating processes  
61 related to the Mediterranean Outflow Water (MOW). After leaping the shallow sill (< 300 m deep) of  
62 the Strait of Gibraltar, the salty and warmer MOW sinks sharply into the deep GoC (depths up to 4000  
63 m), and spreads at depths between 800 and 1200 m, where it finds the equilibrium in the gravitational  
64 field (Sanchez et al, 2017). However, a shallow vein detaches and flows at depths as shallow as 400 m  
65 or less along the northern continental slope of the GoC, turning poleward around the CSV (Ambar 1983;  
66 Cardeira et al., 2013).

67 The higher level of salt entering the North Atlantic through the Strait of Gibraltar and how it spreads  
68 throughout the Atlantic basin is a key factor with implications in the functioning of the Atlantic  
69 Meridional Overturning Circulation (AMOC), and therefore with climatic consequences. Due to the  
70 water column stability, diapycnal mixing of the MOW through entrainment occurs at long time scales  
71 when compared with horizontal dispersion through advection (Mauritzen et al, 2001). MOW is  
72 dominated by a succession of mesoscale rotating structures, the so called meddies (Mediterranean  
73 eddies) (Bower et al., 1995; Ambar et al., 2008). Meddies are described as rotating salt-water lenses,  
74 typically 50-200 km wide and 100-200 m thick. There is some evidence that the dynamic effect of  
75 meddies propagate along the entire water column, till the surface (Serra et al, 2010). CSV is identified  
76 as a site for meddy generation. Topographic features along the continental slope near CSV are  
77 hypothesized as meddy triggers. The key role that the CSV region plays in a wide variety of  
78 oceanographic processes of all scales, some impacting the entire North Atlantic circulation,  
79 demonstrates the relevance of the region to install a high-resolution subsurface observatory.

## 80 **2. Motivation and Objectives**

81 In the frame of the European Multidisciplinary Seafloor and water column Observatory – European  
82 Research Infrastructure Consortium (EMSO-ERIC – <https://emso.eu/>) physical and biogeochemical  
83 data from fixed ocean observation platforms throughout Europe are aggregated, harmonized, and  
84 shared openly under the Creative Commons Attribution License (CC-BY) license, guaranteeing open  
85 access for anyone. EMSO-ERIC is a distributed research infrastructure, encompassing observatories  
86 and test sites along European waters, from coastal to deep sea locations. Some observatories have  
87 already been operating for some time, whereas other nodes are yet to be established.

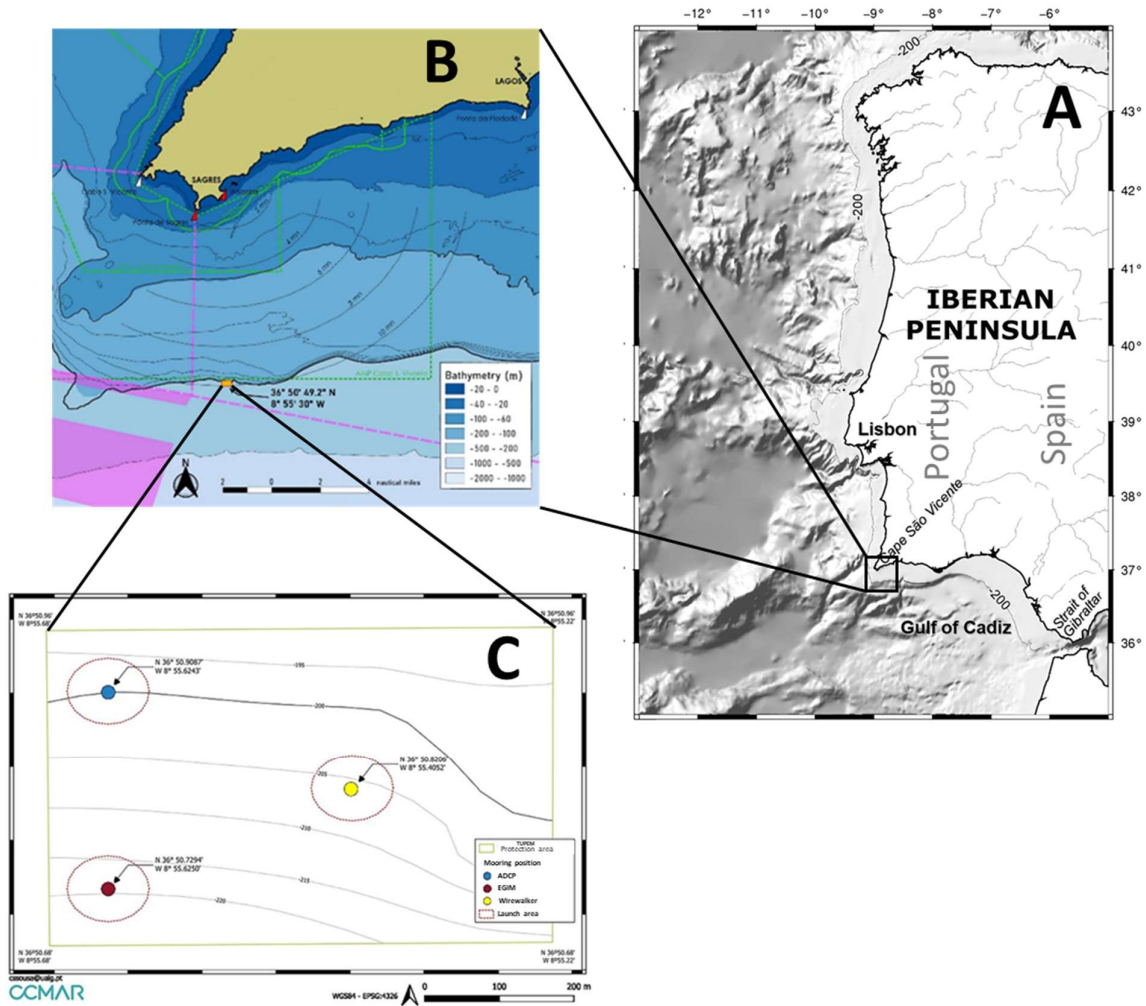
88 The EMSO-ERIC initiative defined the Iberian margin, specifically the region southwest of the CSV,  
89 as the location to install a regional facility of its European network. Along with other objectives  
90 related to geo-hazards seafloor observations, this was the opportunity to carry out long term *in situ*  
91 observations of the subsurface ocean in a clearly under sampled area, regarding its oceanographic  
92 relevance. In the region, *in situ* observations are limited to event scale records from research cruises.  
93 Therefore, the main goal was to construct continuous high resolution and long-term time series of  
94 oceanographic variables along the water column. A mobile platform carrying oceanographic sensors,  
95 moving continuously throughout the water column, robust enough to survive the energetic seas of the  
96 region for long periods, was carefully selected. The vertical definition of the flow field would be  
97 ensured by placing an acoustic doppler current profiler (ADCP) nearby, sampling the entire water  
98 column. The EMSO-Iberian Margin - Cape São Vicente observation platform (IbMa-CSV) is currently  
99 producing the first long term set of observations, from which the seminal deployment data are  
100 presented in this article.

101 While, *in situ* observations play a major role in understanding ocean dynamics and can be used for  
102 various purposes, until today the availability of continuous and long-term *in situ* data of the ocean is  
103 sparse. The construction of long high-resolution time-series is fundamental to access the long-term  
104 physical and biogeochemical variability of the water column, and to improve modeling efforts, meeting  
105 climatic change and ecosystem functions objectives. The data gathered are highly valuable for the  
106 scientific community, with social and economic implications. Most political decisions are taken based  
107 on evidence or future scenarios, mainly provided by numerical models. Due to the turbulent nature of  
108 the ocean flow, numerical models need to be parametrized. More accurate parameterizations are  
109 achieved when based on *in situ* observations, the higher the resolution the better, resulting in more  
110 realistic numerical models. Therefore, one of the criteria that drove the choice of the observation devices  
111 to install at IbMa-CSV was the generation of high-resolution records.

### 112 **3. Methods**

#### 113 *3.1 The EMSO-Iberian Margin Cape São Vicente observatory (IbMa-CSV) - setup and operation*

114 The IbMa-CSV is located at the southwestern tip of the Iberian Margin, 10 nm south of CSV, on the  
115 edge of the continental shelf (approximately 200 m depth). Deployment site selection carefully  
116 considered fishing activity in the surrounding area, avoiding well known heavy equipment preferred  
117 routes (e.g. trawling, longlines). A Permit for Private Use of the National Maritime Space (TUPEM)  
118 was authorized by the Directorate-General for Natural Resources (DGRM) for an area of 0.35 km<sup>2</sup>, in  
119 which the observatory is deployed and should not be entered by other parties. However, ship traffic and  
120 fishing activities pose a significant risk to the observatory as the TUPEM area is not patrolled. To  
121 minimize this risk, engagement actions were undertaken with local communities and the legal  
122 concession publicized in local navigation charts through official channels. This approach proved to be  
123 successful as there was no visible and/or reported incident. The boundaries of the TUPEM area are  
124 N36°50.9087' W8°55.6243', N36°50.9600' W8°55.2200', N36°50.6800' W8°55.6800' and  
125 N36°50.6800' W8°55.2200'. Within this area the instruments are fixed on three separate moorings  
126 (Figure 1C). The TUPEM is managed by the Algarve Centre of Marine Sciences (CCMAR), Faro,  
127 Portugal.



128

129 **Figure 1.** Location of the CSV region (A). Reserved TUPEM , managed by the CCMAR. IbMa-CSV is located within the  
 130 TUPEM area (B). Mooring sites for each platform; vertical wave-powered profiler (surface, yellow), EGIM (subsurface, red),  
 131 ADCP (subsurface, blue) (C).

132 Mooring design followed current best practices (e.g. Coppola et al., 2016), based on two  
 133 platform types: subsurface (EGIM and ADCP), and surface (vertical profiler). The subsurface  
 134 moorings were conceived as linear structures from anchor to buoy, while the surface mooring  
 135 was based on an inverse catenary configuration. The choice of the hardware to be used in the  
 136 mooring, i.e. the size and shape of the anchor, the type of rope and chain, number, size and  
 137 shape of flotation aids and their position along the mooring line, linking hardware (shackles,  
 138 swivels, d-links), were all carefully considered to meet the environmental features of the  
 139 deployment area (e.g. waves, atmospheric forcing, presence of strong currents). Static and  
 140 dynamic behavior of all three designs was then simulated in a dedicated software (Proteus DS),  
 141 considering time dependent forcing parameters (wind, currents and waves) to evaluate vertical  
 142 load, components position, tilt and tension, required safe anchor mass, and overall mooring  
 143 configuration, according to different set scenarios, i.e. “normal”, “storm”, and “extreme”.

144 Moorings were required not only to endure “extreme” conditions without failure, but also  
145 maintain operational capabilities (to a reasonable extent) under more energetic events.  
146 Simulated results pointed to neglectable instrumentation tilt of the subsurface moorings under  
147 a set maximum 0.6 m/s current. Regarding the surface mooring, vertical travel wire inclinations  
148 greater than 20° were expected to hinder vertical motion. Simulated inclinations were on  
149 average 5.7°, 15.2°, and 29.5°, under “normal”, “storm” and “extreme” scenarios, respectively,  
150 as such considered to be satisfactory. Operating depths, i.e. the subsurface platforms placed  
151 broadly below 150 m depth, and the vertical profiler travelling between approximately 150 m  
152 and 1 m in constant motion (~5 or 6 full profiles per hour), were expected to deter significant  
153 biofouling growth, requiring as such minor control techniques, such as a homespun coating  
154 applied to the ADCP transducers (zinc oxide paste mixed with cayenne pepper), as well as  
155 copper tape around the optical sensors. Recovered equipment experienced, as expected,  
156 biofouling, however, while the ADCP subsurface platforms were unaffected, the vertical  
157 profiler was compromised after the two months, where algae growth led to the salinity sensor  
158 operation hinderance. Based on these findings, a new strategy must be developed for future  
159 deployments, whether it is to clean the sensors regularly during the deployment period or using  
160 innovative biofouling control techniques compatible with available sensors (wipers, non-toxic  
161 coating, UV lights, for instance)

### 162 *3.2 Data acquisition platforms and settings Instruments, parameters, and sampling*

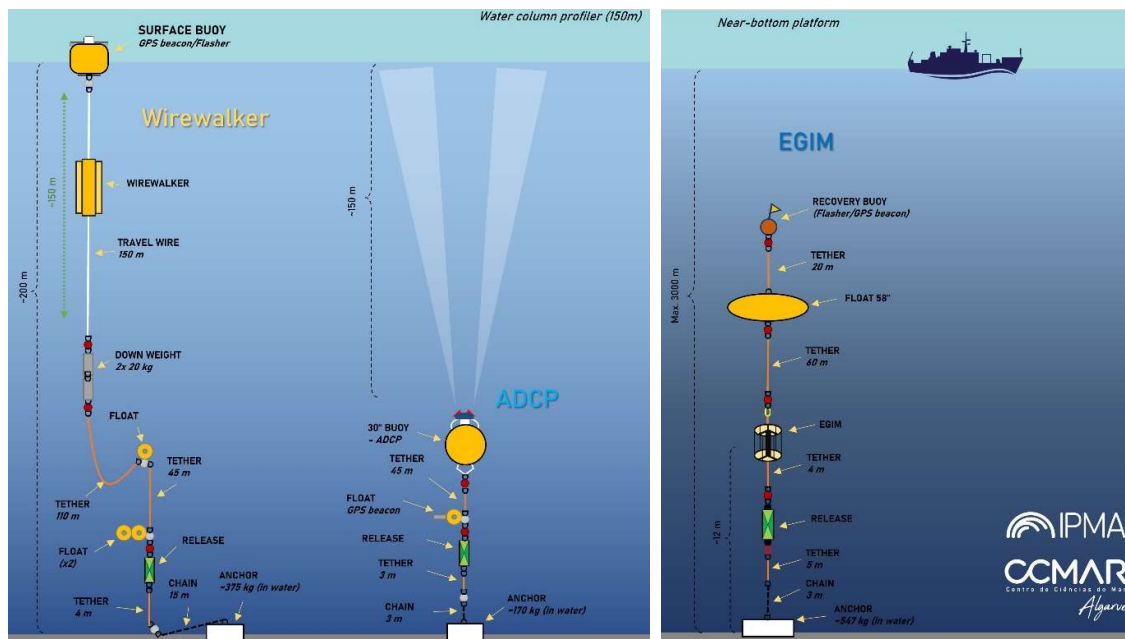
163 An ADCP (Teledyne RDI Sentinel V100 300 kHz), mounted in a upward facing subsurface buoy  
164 (36.848478 N , -8.927072 E; 150 m), a vertical wave-powered profiler (Wirewalker) (36.84701 N, -  
165 8.92342 E; near surface to 150 m), and an EMSO Generic Instrument Module (EGIM) (36.84549 N, -  
166 8.927083 E; 200 m) were deployed from the R/V Mário Ruivo during the EMSO-PT Leg 2 Campaign,  
167 in collaboration with the Portuguese Institute for the Sea and Atmosphere, I.P. (IPMA, I.P.), in the  
168 TUPEM area during June – October 2022 (Figure 2).

169 ADCP data were collected every hour for 3 m depth bins (51 bins in total), mounted at 150 m depth  
170 (Figure 3). The blank right above the ADCP accounts for 2 m. Ping interval was 1 s and number of pings  
171 120. East-west and north-south component ( $\text{ms}^{-1}$ ) of the current together with the magnitude and  
172 direction were acquired. Supplemental parameters, substantial for quality control, are provided  
173 additionally, including correlation, echo intensity and percent of good return of each of the four beams,  
174 as well as heading, pitch, and roll. The ADCP was further equipped with a thermistor and pressure  
175 sensor. The ADCP was calibrated before the deployment according to manufacture guidelines.

176 A 6 channel RBRconcerto CTD, equipped with two Turner Designs Cyclops 7F sensors (Chl-a and  
177 Turbidity) and one RBRcoda3 T.ODO (optical dissolved oxygen) were installed in a vertical wave-

178 powered vertical profiler, travelling from about 1 m below surface to 150 m depth at an variable speed:  
 179 upward cast (free floating)  $\sim 0.5 \text{ ms}^{-1}$ ; downward cast (wave motion)  $\sim 0.4 \text{ ms}^{-1}$  (depending on wave  
 180 conditions). Sampling rate was 2 Hz ascending, and 10 s descending. Measured channels were  
 181 conductivity, temperature, pressure, chlorophyll-a, dissolved  $\text{O}_2$  concentration, and turbidity. Derived  
 182 channels are sea pressure, depth, salinity, speed of sound, specific conductivity, dissolved  $\text{O}_2$  saturation,  
 183 and density anomaly.

184 The EGIM, equipped with a SeaBird SBE37, Aanderaa 4831dw, RBRquartz 3 BPR, WETLabs ECO-  
 185 NTU, OCEANSONICS icListen SB60L-ETH and Teledyne RDI 300kHz Workhorse Monitor direct-  
 186 reading ADCP, was fixed at approximately 200 m depth.



187  
 188 **Figure 2.** Schematic representation of the IbMa-CSV platforms. Left: Vertical wave-powered profiler and ADCP moorings,  
 189 managed by CCMAR. Right: EGIM mooring, managed by IPMA and CCMAR.

190 Sampling period was 60 minutes (ADCP), 15 minutes (CT, Turbidity, Oxygen), 30 seconds (Pressure),  
 191 and 5 minutes / 1 minute recording (acoustics). Measured channels include conductivity, temperature,  
 192 pressure, temperature, dissolved  $\text{O}_2$  concentration, turbidity, currents, and passive acoustics. Derived  
 193 channels are sea pressure, depth, salinity, speed of sound, specific conductivity, dissolved  $\text{O}_2$  saturation,  
 194 and density anomaly. The data time-series from the ADCP and the Wirewalker, managed by CCMAR,  
 195 will be presented in this data paper, along with the description of the data processing and results.

#### 196 4. Data files and metadata

197 Instrument data files come in comma-separated value files and are converted into NetCDF format  
 198 according to CF Conventions 1.6. Files are named after facility code, platform code (WW, EGIM),  
 199 deployment number (D01, D02, ..., Dnn), deployment period, and version (v001, v002, ..., vnnn) e.g.  
 200 [folder\_path]IBMA-CSV\_WW\_D01\_yyyymmdd\_to\_yyyymmdd\_v001.nc. Changes are tracked in a

201 log-text file, which is located in the “dataset type” – directory. Instrument data (raw) are identified with  
 202 the code “\*\_v001” and metadata with code “\*\_M”.

203 The vertical wave-powered profiler data are divided into six NetCDF files, each one approximately two  
 204 million data points, to keep file size reasonable. Each NetCDF is built upon the same structure: Global  
 205 attributes, Dimensions and Variables. Global attributes describe the dataset universally through a short  
 206 descriptive summary as well as other attributes such as temporal extension, geospatial position, principal  
 207 investigator, person of contact and more (Table 1). Each variable is embedded in one or more  
 208 dimensions, in this case: Time, Longitude, Latitude, Depth and Bins. Each parameter is accompanied  
 209 by a set of metadata attributes, holding detailed information about the instrument type, the units and  
 210 other relevant information regarding the variable. The SeaDataNet parameter discovery vocabulary  
 211 (<https://vocab.seadatanet.org/search>), well established in ocean science, is used for attributes,  
 212 dimensions, variables and units. Further, vocabulary is based on the Copernicus Marine Environment  
 213 Monitoring Service *In Situ* Thematic Assembly Centre (CMEMS INSTAC) Manual v3.2 and  
 214 SeaDataNet OceanSITES Data Format Reference Manual v1.4. Common vocabulary facilitates  
 215 machine-readability and manual findability by users. Each dataset is accompanied by comprehensive  
 216 metadata. Global and variable specific metadata attributes were agreed upon in the Data Management  
 217 Service Group (DMSG) of EMSO-ERIC (Table 1). The main objective of EMSO-ERIC DMSG is to  
 218 make each dataset as findable, accessible, interoperable and (re)usable as possible, according to FAIR  
 219 standards, harmonize data quality control, format and metadata procedures. Each in this data paper  
 220 presented dataset can be reused under the CC-BY 4.0 license (<https://spdx.org/licenses/CC-BY-4.0>).

221 **Table 1.** EMSO-ERIC Data Management Service Group Metadata Catalogue.

Global Attributes	Dimensions	Variables	Quality Control
date_created	long_name	long_name	long_name
Conventions	standard_name	standard_name	flag_values
institution_edmo_code	units	units	flag_meanings
institution_edmo_uri	axis	comment	conventions
insitution_ror_uri	ancillary_variables	coordinates	
geospatial_lat_min	sdn_parameter_name	ancillary_variables	
geospatial_lat_max	sdn_parameter_urn	sdn_parameter_name	
geospatial_lon_min	sdn_uom_name	sdn_parameter_urn	
geospatial_lon_max	sdn_uom_urn	sdn_parameter_uri	
geospatial_vertical_min		reference_scale	
geospatial_vertical_max		sdn_uom_name	
time_coverage_start		sdn_uom_urn	
time_coverage_end		sdn_uom_uri	
update_interval		sensor_model	
site_code		sensor_reference	
emso_facility		sensor_type_uri	
source		sensor_type_name	



platform_code		sensor_manufacturer	
wmo_platform_code		sensor_manufacturer_uri	
data_type		sensor_serial_number	
format_version		sensor_mount	
network		sensor_orientation	
data_mode		sensor_depth	
title		QC_indicator	
summary			
keywords			
keywords_vocabulary			
project			
principal_investigator			
principal_investigator_email			
doi			
references			
license			
license_uri			

222

223 Quality control variables were created for each measured parameter and for some derived parameters.  
 224 The quality control variable name is composed of the variable name of the parameter and the suffix  
 225 “\_QC”. Quality control procedures and flagging conventions are described in further detail in the next  
 226 section. For each dataset it was assured that solely measurements conducted in the water column were  
 227 considered. This was achieved by examining depth measurements, derived from the pressure sensor as  
 228 well as temperatures indicating atmospheric temperatures. Out of water values were removed from each  
 229 dataset.

### 230 **5. Technical Validation**

231 Each dataset was subject to quality control (qc). Suspicious and bad values were not removed from the  
 232 published raw dataset. Instead, a complimentary qc-variable was created, holding flag values describing  
 233 each individual parameter value. Flag values are defined by the OceanSITES Data Format Reference  
 234 Manual v1.4 (OceanSITES, 2020). Flag may take the values 0, 1, 2, 3, 4, 7, 8, 9 that are defined as  
 235 “unknown”, ”good\_data”, “probably\_good\_data”, “potentially\_correctable bad\_data”, “bad\_data”,  
 236 “nominal\_value”, “interpolated\_value”, “missing\_value”, respectively. Suspicious and bad values were  
 237 flagged as “potentially\_correctable bad\_data” (3) and “bad\_data” (4), respectively.

238 Contrary to the published raw dataset, this paper presents the quality controlled data. Data flagged as  
 239 “potentially\_correctable bad\_data”, “bad\_data” and “missing\_value” were excluded from the plots  
 240 presented in this manuscript.

241 ADCP quality control was based on the quality control procedures from Garel *et. al.* (2016). To ensure  
 242 that no data subject to site lobe interference is shared, the upper 10 % of the data was flagged as

243 “bad\_data”. Further, the sea surface was detected by locating the cells with a difference among adjacent  
244 values greater than three and flagged bad accordingly. This criterion was restricted to cells above the  
245 14<sup>th</sup> cell (100 m) to prevent misinterpretation of the surface. Cells above and the cell immediately below  
246 were flagged as “bad\_data”. Furthermore, if two or more beams with cells featuring a difference among  
247 adjacent bins in echo intensity > 30, and/or with three or more out of four beams with correlation  
248 magnitude values lower 64 counts were also flagged as “bad\_data”. Temperature was controlled  
249 according to SeaDataNet Guidelines (see above), and pressure was assessed via visual inspection.

250 The first quality control check for the vertical profiler data was done visually via line and boxplots of  
251 each variable, allowing a global and regional range check and spike detection at first sight. Quality tests  
252 applied on each variable of this dataset were: Sensor range test, global range test, regional range test and  
253 spike test. A gradient test was additionally applied to temperature and salinity. Global ranges were  
254 obtained from literature for each variable, whereas regional ranges were discussed and selected with the  
255 support of experts from the region.

256 Temperature and salinity Spike Test (ST) was conducted according to SeaDataNet Data Quality Control  
257 Procedures Manual (SeaDataNet 2010), using the following algorithm: Test value =  $|V_2 - (V_3 + V_1)/2$   
258  $- | (V_3 - V_1) / 2 | > V\_THRESHOLD$ . The value is flagged “bad\_data” when the test value exceeds  
259 6 °C, 0.9 PSU, respectively. Gradient Test (GT) relied on the following from SeaDataNet proposed  
260 algorithm: Test value =  $(|V_2 - (V_1 + V_3)/2| > V\_GRAD$ . The value is flagged “bad\_data” when the  
261 test value exceeds 9 °C, 1.5 PSU, respectively. Spikes in conductivity were determined by Interquartile  
262 Range Test (IQR) (Hald, 1952). Quartile two and quartile three make up the interquartile range (IQR)  
263 of the data. Two thresholds are defined for “suspicious” (1.5) and “bad\_data” (3). The IQR is multiplied  
264 by each threshold and subtracted (added) from quartile 1 (quartile 3). If a data point exceeds the  
265 computed range, it is flagged accordingly. A IQR test was not applied on other variables as it was found  
266 to be overly sensitive to biogeochemical variables, discarding reasonable values. Therefore, other  
267 manuals and standards were used for spike detection in biogeochemical parameters.

268 Dissolved oxygen, alongside with oxygen saturation, were assessed based on the ST proposed in the  
269 Manual for Real-Time Quality Control of Dissolved Oxygen Observations by the Integrated Ocean  
270 Observing System (IOOS) Quality Assurance / Quality Control of Real Time Oceanographic Data  
271 (QUARTOD) (IOOS QUARTOD, 2018). A spike reference (average of adjacent points  $DO_{n-2}$  and  $DO_n$ )  
272 is subtracted from the tested value ( $D_{n-1}$ ) and tested against an upper and lower threshold. Values failing  
273 the upper boundaries are flagged as “bad\_data”, values in the range of the lower and upper threshold are  
274 flagged as “suspicious”. Thresholds for dissolved oxygen and oxygen saturation were set at 4 mg/l-1  
275 (lower) and 8 mg/l-1(upper) and 80 % (lower) and 120 % (upper), respectively. The most reliable  
276 chlorophyll-a spike detection for this dataset is proposed by The Platforms for Biogeochemical studies:  
277 Instrumentation and Measure (PABIM) (PABIM, 2010). The ST algorithm remains the same as in the  
278 SeaDataNet Guidelines for temperature and salinity. PABIM (PABIM, 2010) suggests an algorithm to

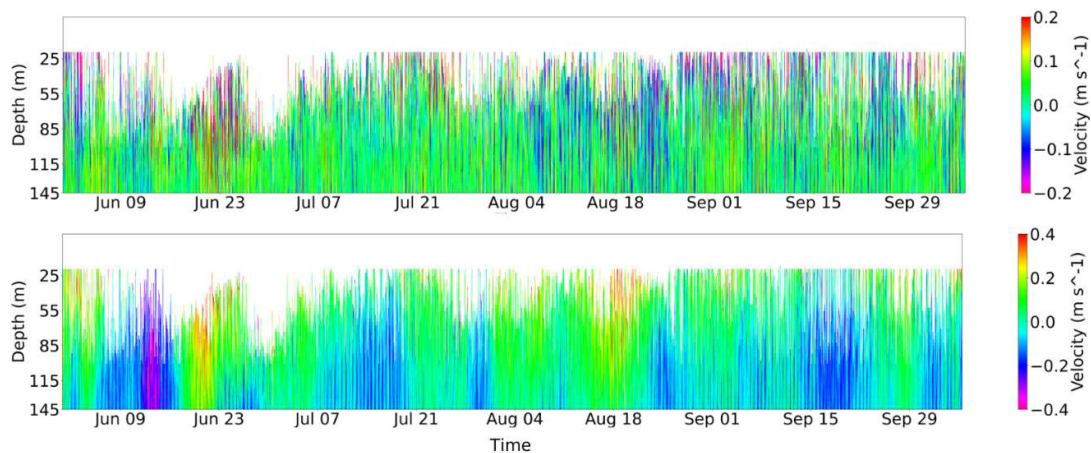
279 define the threshold value, most appropriate in any region, which is computed as follows:  
 280  $\text{Threshold\_Value} = |\text{median}(V_0, V_1, V_2, V_3, V_4)| + |\sigma(V_0, V_1, V_2, V_3, V_4)|$ . Turbidity spikes are detected  
 281 with the same methodology as chlorophyll-a, using a predefined threshold of 6 NTU.

## 282 6. Data Records

283 In this section we visualize the entire data series of the vertical profiles of the of the measured and  
 284 derived variables in a comprehensive way. Only validated data are displayed. Data considered as bad or  
 285 potentially bad were not considered to display or for the interpolations, as stated in the previous section.  
 286 Preliminary analyses as well as basic statistics are presented.

### 287 6.1 Acoustic Doppler Current Profiler

288 Current data from the upward facing ADCP were acquired from June to October 2022 at a depth of 150  
 289 m (Figure 3). Measurements above 10 m failed the quality control criteria due to interference with the  
 290 surface resulting in biased data and were discarded. In the plots we present only the data below 20 m  
 291 deep (Figure 3).



292

293 **Figure 3.** Meridional (north-south) (**top**) and zonal (east-west) (**bottom**) component of acoustic doppler current profiler  
 294 throughout the whole water column from June to October 2022. White patches reveal absence of valid data. Negative values  
 295 indicate southward (westward) flow, whereas positive values indicate northward (eastward) flow direction. Measurements are  
 296 expressed in  $\text{ms}^{-1}$ . Data above approximately 20 m suffer from surface interference and were removed.

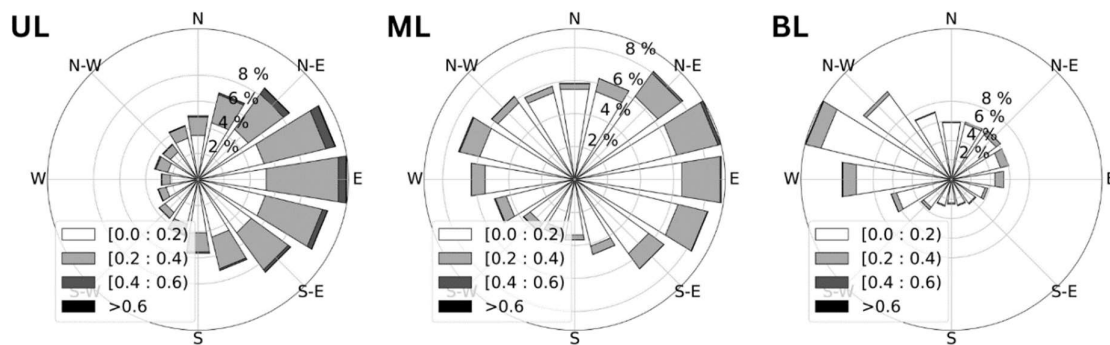
297

298 Current meter records demonstrate an energetic current regime in the area south of CSV. Clearly, the  
 299 dominant flow is zonal. The meridional component is weak, without any clear tendency in the direction  
 300 (notice the different scales of the velocity in Figure 3). The zonal flow shows a prevailing eastward flow,  
 301 interleaved with sudden inversions to westward. Westward flows are more frequent towards the seafloor.

302 Current meter records were divided into three depth ranges to understand the distinctive current regimes  
 303 along the vertical. The upper layer (UL) comprises the surface waters, reaching down to 60 m. The  
 304 middle layer (ML) of the water column ranges from 60 to 100 m, and the bottom layer (BL) covers from

305 100 to 150 m. Polar plots were created for each depth layer to depict the vertical change of the magnitude  
 306 and direction of the flow (Figure 4). A relatively energetic flow, showing a few episodes of increased  
 307 velocities  $> 0.75 \text{ m s}^{-1}$ , prevails in the upper layer. There, the flow shows a strong eastward component,  
 308 contrasting with the almost absence of westward flow. In the middle layer this prevalence diminishes,  
 309 and the flow intensity decays, with velocities sporadically reaching values  $> 0.6 \text{ m s}^{-1}$ , but mostly ranging  
 310 between  $0.001 - 0.4 \text{ m s}^{-1}$ . As we approach the seafloor, in the bottom layer, the flow is weak, with  
 311 velocities between  $0$  and  $0.2 \text{ m s}^{-1}$ , and a prevailing westward component is evident, opposed to the  
 312 upper ocean layer. A basic statistic of the flow velocity for each depth interval is presented too.

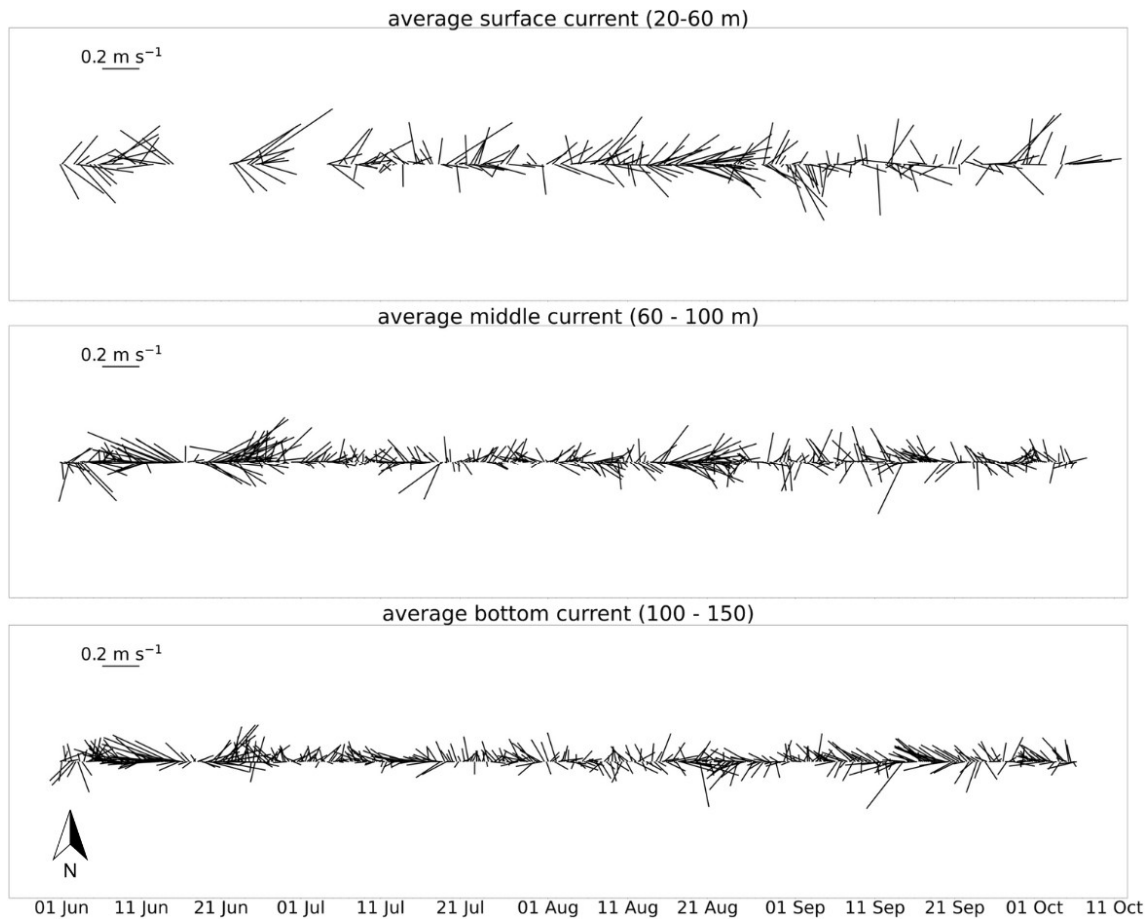
313



314

315 **Figure 4.** Demonstration of current magnitude and direction of the upper layer (UL; 10 - 60 m), middle layer (ML; 60 -  
 316 100m), bottom layer (BL; 100 - 150 m).

317 To detail the temporal variability of the mean flow in each depth layer, stick diagrams are presented for  
 318 each depth layer (Figure 5). The intensified current in the upper layer can be observed throughout the  
 319 whole period of the deployment. A more diffuse pattern in direction, along with the decrease in velocity  
 320 can be observed in the lower layers, except for a short period during mid-June. However, there is a  
 321 prevalence of zonal flow, interrupted periodically by momentary direction changes. June can be  
 322 identified as the most energetic month in the time series, featuring the highest mean values throughout  
 323 the water column.



325

326 **Figure 5.** ADCP stick plot from June to October 2022 divided into upper layer (20-60 m; top), middle layer (60-100 m; middle)  
 327 and bottom layer (100-150 m; bottom).

328 **Table 2.** Statistics of upper layer (UL; 10-60 m), middle layer (ML; 60-100 m) and bottom layer (BL; 100-150 m) grouped  
 329 by month. SD representing the standard deviation. Values are expressed in ms<sup>-1</sup>.

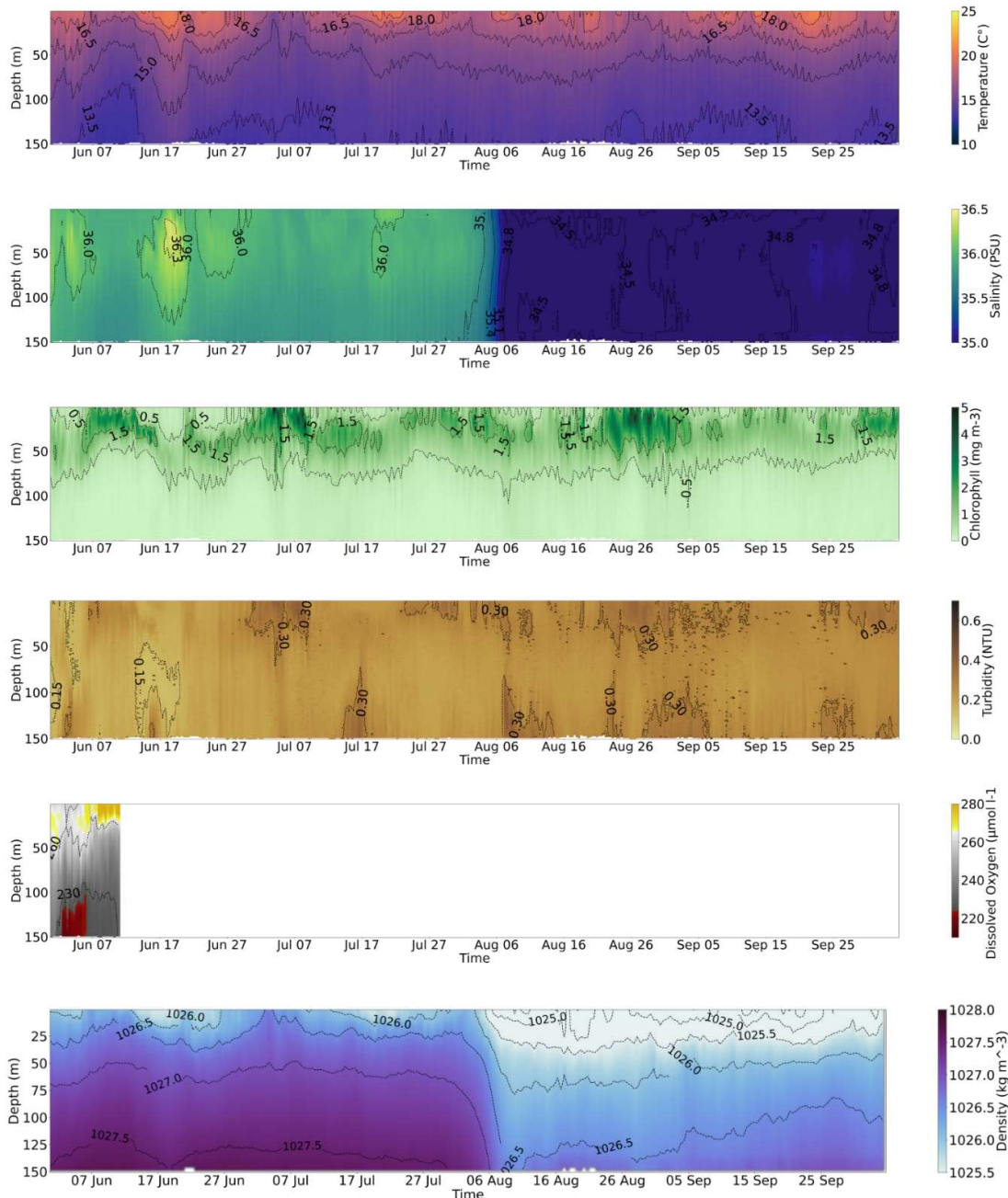
	UL				ML				LL			
	Mean	SD	Min	Max	Mean	SD	Min	Max	Mean	SD	Min	Max
<b>June</b>	0.247	0.105	0.009	0.773	0.186	0.095	0.004	0.574	0.142	0.080	0.001	0.687
<b>July</b>	0.142	0.078	0.002	0.730	0.100	0.059	0.001	0.787	0.089	0.047	0.000	0.509
<b>August</b>	0.182	0.096	0.001	0.639	0.125	0.074	0.000	0.469	0.098	0.053	0.001	0.385
<b>Sept</b>	0.151	0.096	0.003	0.716	0.107	0.059	0.001	0.600	0.101	0.058	0.002	0.510

330

### 6.2 Vertical wave-powered profiler

331 Continuous time series of the entire water column are highly valuable as they offer vast amounts of data  
 332 and can create a comprehensive picture of mesoscale and sub-mesoscale processes. The vertical wave-  
 333 powered profiler, equipped with physical and biogeochemical sensors, operated for four months  
 334 continuously, and delivered a rich dataset at the end of the deployment. Vertical profiles of the water  
 335 column show temperatures between 12.5 °C closer to the seafloor to approximately 22 °C on the surface  
 336 (Figure 4; Table 3). The thermocline remains between 20-40 m, showing some periods of a well-mixed  
 337 homogenous surface layer and periods of more stratified waters (Figure 4; Figure 5). Salinities are found

338 to range between 33 and 37 from June to the end of July with an average salinity of 35.95 (SD  $\pm$ 0.13)  
339 and 35.88 (SD  $\pm$ 0.09), respectively (Figure 4; Table 3). Salinity data beyond that point were discarded  
340 and will not be discussed further as the conductivity sensor was subject to intense biofouling, prohibiting  
341 the collection of trustworthy measurements after the month of July. Due to that the mixed layer depth  
342 was only computed for the months of June and July, showing an average Mixed-Layer Depth (MLD)  
343 around the 10-20 m mark, following the pattern of the thermocline (Figure 8, top). The dissolved oxygen  
344 sensor shows lower oxygenated waters in deeper waters but stopped operating after two weeks (Figure  
345 4). The chlorophyll-a maximum can be found between 20-60 m with concentrations between 1-10 mg  
346  $\text{m}^{-3}$  and mitigates to almost 0  $\text{mg m}^{-3}$  below (Figure 6; Figure 5; Table 3). Turbidity concentrations  
347 correspond to chlorophyll-a during the whole course of the measurements, with average concentrations  
348 of 0.25 NTU (SD  $\pm$ 0.17), indicating the correlation between turbidity and biomass with some additional  
349 phases of increased turbidity concentrations close to the seafloor (Table 3).



351

352 **Figure 4.** Continuous vertical wave profiler data Jun-Oct 2022. **Top to bottom:** Temperature ( $^{\circ}\text{C}$ ), salinity, chlorophyll-a  
 353 concentration ( $\text{mg m}^{-3}$ ), turbidity (NTU), dissolved oxygen ( $\mu\text{mol l}^{-1}$ ), and density ( $\text{kg m}^{-3}$ ). Salinity and density values after  
 354 the month of July are ambiguous and are discarded from further discussion.

355 In June two period of increased salinity were recorded between the 1<sup>st</sup> – 6<sup>th</sup> and 13<sup>th</sup> to the 21<sup>st</sup> of June  
 356 near the surface down to 120 m depth, together with mitigation in chlorophyll-a concentration, migrating  
 357 to deeper layers along the mixed layer to a depth of approximately 60 m (Figure 4; Figure 6). The salty  
 358 waters appear in form of an isolated lens, carrying maximum salinities of 36.72 (Figure 4; Figure 5).  
 359 Simultaneously, an intensification in stability and spiciness can be observed (Figure 6). Spiciness was

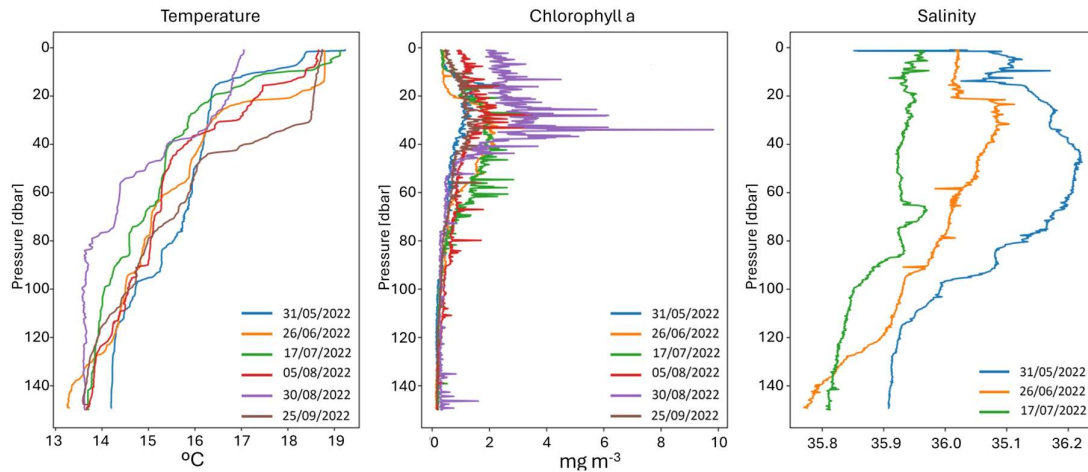
360 computed with the Thermodynamic Equation of Seawater 2010 (TEOS-10) from Absolute Salinity and  
 361 Conservative Temperature, according to McDougall and Krzysik (2015).

362 Table 3. Statistics of vertical wave-powered profiler parameters grouped by month. SD representing the standard deviation.  
 363 Recordings are lacking for the variables dissolved oxygen, oxygen saturation after the first half of June and for salinity after  
 364 July.

	June				July			
	Mean	SD	Min	Max	Mean	SD	Min	Max
Temperature (°C)	15.55	1.97	12.62	21.3	15.15	1.7	12.64	20.51
Conductivity (S m <sup>-1</sup> )	4.46	0.21	4.13	5.06	4.41	0.18	4.14	4.98
Salinity	35.95	0.13	34.44	36.72	35.88	0.09	34.13	37.02
Dissolved Oxygen (µmol l <sup>-1</sup> )	245.35	18.5	209.96	305.46	-	-	-	-
Oxygen Saturation (%)	97.77	10.5	81.08	120.0	-	-	-	-
Chlorophyll a (mg m <sup>-3</sup> )	0.59	0.65	0.08	9.33	0.76	0.81	0.09	10.84
Turbidity (NTU)	0.2	0.07	0.0	6.17	0.25	0.09	0.0	6.42
Sound velocity (m s <sup>-1</sup> )	1510.48	5.43	1502.08	1526.23	1509.22	4.62	1502.31	1524.2
	August				September			
	Mean	SD	Min	Max	Mean	SD	Min	Max
Temperature (°C)	15.41	1.64	12.64	21.56	15.48	2.03	12.74	21.22
Conductivity (S m <sup>-1</sup> )	4.31	0.16	4.01	4.88	4.32	0.19	4.02	4.90
Salinity	-	-	-	-	-	-	-	-
Dissolved Oxygen (µmol l <sup>-1</sup> )	-	-	-	-	-	-	-	-
Oxygen Saturation (%)	-	-	-	-	-	-	-	-
Chlorophyll a (mg m <sup>-3</sup> )	0.83	0.88	0.09	10.51	0.61	0.58	0.08	9.40
Turbidity (NTU)	0.27	0.10	0.04	7.13	0.27	1.41	0.03	363.77
Sound velocity (m s <sup>-1</sup> )	1508.76	4.35	1500.69	1524.31	1508.89	5.44	1501.0	1524.69

365  
 366 Throughout the first half July colder and less saline waters shoal towards the surface with average values  
 367 of  $14.83 \pm 1.44$  °C and  $35.87 \pm 0.07$ , respectively (Figure 4), resulting in a well-mixed and homogenous  
 368 water column. In response, stability and spiciness decrease (Figure 6), accompanied by increasing  
 369 chlorophyll-a concentration ( $0.9 \pm 1.03$  mg m<sup>-3</sup>) and turbidity ( $0.26 \pm 0.07$  NTU). In the second half of  
 370 the months surface waters experience warming and average increase slightly up to  $15.40 \pm 1.83$  °C,  
 371 along with an increased stability and spiciness (Figure 4; Figure 6). Stratification enhances during  
 372 August due to a deepening of the warmer surface waters to a depth of approximately 60 m (Figure 6).  
 373 Around the 24<sup>th</sup> of August colder temperate waters shoal towards the surface (19.4 °C), simultaneously  
 374 with an inflation of the maximum chlorophyll-a concentration (10.51 mg m<sup>-3</sup>), attenuating in the  
 375 beginning of September. Upper layer stratification stabilizes throughout the month of September, with  
 376 temperatures around 21 °C in the upper 40 m with an increased period of warming between the second  
 377 and third week of the month along with a slight decrease of chlorophyll-a (Figure 4). The same pattern  
 378 was observed during mid-August, in which, with increased surface temperatures, higher chlorophyll-a  
 379 concentrations migrate to deeper layers, similar to the third week of July.



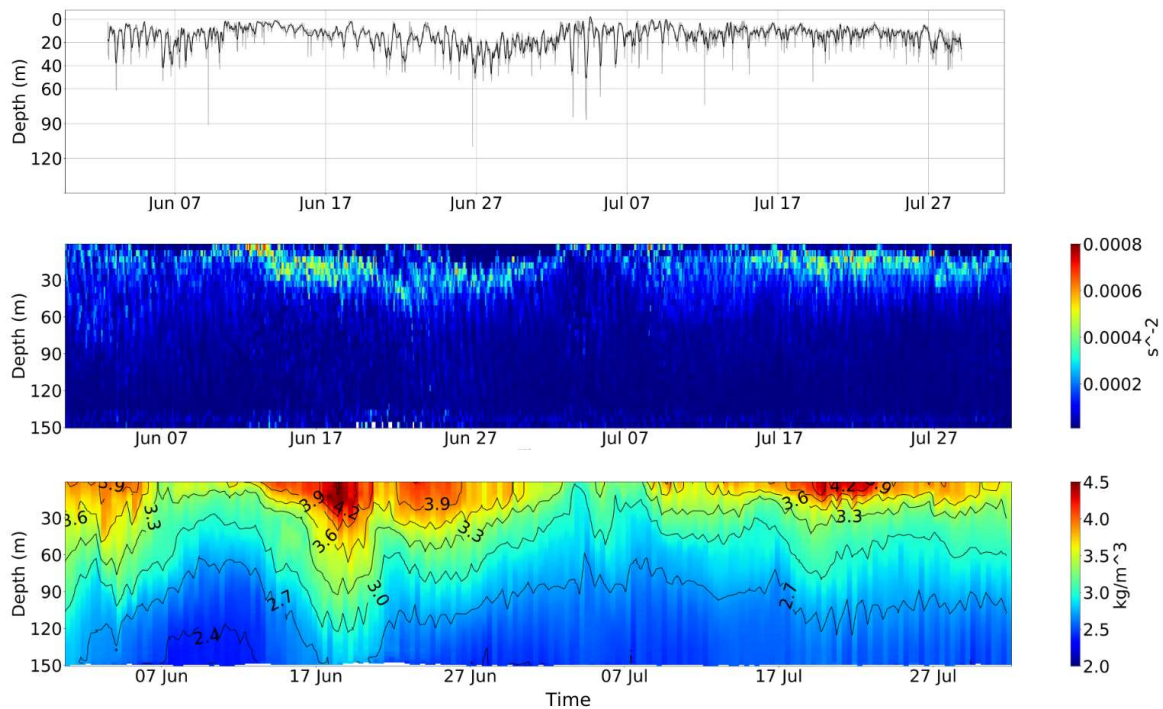


380

381

382

**Figure 5.** Examples of individual vertical profiles of temperature (°C) (**left**), chlorophyll-a (mgm-3) (**middle**) and salinity (**right**).



383

384

385

**Figure 6.** From **top to bottom**: MLD, Brunt-Väisälä frequency ( $N^2$ ), spiciness. Computed for the months of June and July. Subsequent failure of conductivity sensor prohibits computation of presented parameters from that point on.

386

## 7. Data availability

387

388

389

390

391

392

Quality controlled datasets are made publicly available as NetCDF files at the environmental data repository SEANOE (<https://www.seanoe.org/>) under the DOI <https://doi.org/10.17882/94769> in accordance with FAIR principles (Wilkinson et al., 2019). Beyond the repository, data is ingested into the CCMAR Erddap server (<https://erddap.cmar.ualg.pt/erddap/index.html>), in which a first data visualization and data can be downloaded in various file formats selectively from the user. Further, the data is shared with the EMSO-ERIC Data Portal (<https://data.emso.eu/home>), in which users can

393 visualize and download data according to their needs. The data is not restricted and is accessible for  
394 anyone, accompanied with comprehensive metadata. Standardized datasets allow machine readability  
395 and interoperability with various software.

## 396 **8. Data set value**

397 This dataset conveys the importance of continuous, long-term data acquisition and ocean monitoring to  
398 capture mesoscale and sub-mesoscale events in the ocean. As presented before it was detected, for  
399 example during the second half of June, fascinating thermohaline records. This deployment was the first  
400 test run of the IbMa-CSV Ocean Observatory. Sensor failure due to biofouling will be tackled by  
401 following a regular cleaning of the sensors at specific time intervals while deployed (profiler), and by  
402 reducing deployment turn-around with a second vertical wave-powered profiler. Hence, the two profilers  
403 will alternate in a minimum four month rhythm, therefore guarantying a continuous data collection. The  
404 vertical wave-powered profiler offers impeccable high temporal and vertical resolution data products at  
405 reasonable cost and maintenance. The only instruments which provide data products with comparable  
406 resolution are autonomous underwater vehicles and gliders. Yet both economically and regarding the  
407 scope of establishing an Eulerian, long-term observation platform, these instruments cannot compete,  
408 underpinning the exceptional potential of the vertical wave-powered profiler and its data products.

409 The monitoring of energetic areas, such as the western tip of the northern margin of the Gulf of Cadiz  
410 (the CSV), is crucial to understand the complexity of the ocean dynamics and to predict future  
411 development via ocean models and their validation through comprehensive datasets. A wide range of  
412 processes, from the upper layers wind induced upwelling to deeper MOW features, do occur in the ocean  
413 surrounding CSV, as described in the Introduction. Intense mesoscale and sub-mesoscale activity, that  
414 represent the “weather” variability of the ocean imposed by the turbulent nature of the circulation, are  
415 quite conspicuous in this region and dominates all levels of the water column, challenging the  
416 investigation of a wide range of oceanographic processes.

417 Efforts have been made to develop numerical models for this region, with the aim of better  
418 understanding the exchange and mixing processes that occur there, and their implications for the  
419 ecosystem and salt spreading in the North Atlantic. However, there is no general theory of turbulence,  
420 and numerical models must rely on parametrizations to solve this macro-turbulence. The correct  
421 parameterization of the turbulent behavior of the ocean depends on the previous knowledge that we have  
422 about the physical characteristics of the region to be modelled. This knowledge is built upon the  
423 observation of the ocean. Higher resolution observations will produce better parameterizations of the  
424 numerical models. The present knowledge of the oceanography of the region is inferred from event scale  
425 sampling, leading to regional numerical models highly data deficient., that tend to use parameterization  
426 analogies with ocean regions with similar oceanographic characteristics and intensively sampled, such  
427 as the California Upwelling System (Macias et al., 2014; Janeiro et al., 2017). This data series will make

428 it possible to find better parameters for the region and to solve more realistically the turbulence and  
429 turbulence related ocean processes.

430 The present data set, with such vertical and temporal resolution, is unique in the region. The nearest  
431 moorings, operated by the Instituto Hidrográfico (Portugal), are more than 120 km away, and only take  
432 measurements at the surface (<https://www.hidrografico.pt/index/en>). The velocity field is assessed only  
433 at the surface through HFRs that cover the region, operated by the Puertos del Estado (Spain)  
434 (<https://www.puertos.es>) and the Instituto Hidrográfico (Portugal). For the first time the subsurface is  
435 sampled in the region. The high-resolution sampling, covering the surface layer down to a depth of 150  
436 meters, makes this dataset unique in a vast area of the ocean, disclosing the high oceanographic value  
437 of the data set. The IbMa-CSV Ocean Observatory was established in the scope of EMSO-ERIC, a  
438 European wide ocean observatory network, and will be further developed and improved to operate  
439 continuously and long-term.

#### 440 **9. Usage note**

441 EMSO data are published without any warranty, express or implied. The user assumes all risk arising  
442 from the use of EMSO data. EMSO data are intended to be research-quality and include estimates of  
443 data quality and accuracy, but it is possible that these estimates or the data themselves contain errors. It  
444 is the sole responsibility of the user to assess if the data are appropriate for his/her use, and to interpret  
445 the data, data quality, and data accuracy accordingly. EMSO welcomes users to ask questions and report  
446 problems to the contact addresses listed in the data files or on the EMSO web page.

#### 447 **10. Acknowledgement**

448 This study received Portuguese national funds from: FCT - Foundation for Science and Technology  
449 through project UIDB/04326/2020, UIDP/04326/2020 and LA/P/0101/2020; operational programmes  
450 CRESC Algarve 2020 and COMPETE 2020 through projects EMBRC.PT ALG-01-0145-FEDER-  
451 022121 and EMSO-PT ALG-01-0145-FEDER-022231; EEA Grants Blue Growth project "Atlantic  
452 Observatory – Data and Monitoring Infrastructure" (PT-INNOVATION-0002). Furthermore, we would  
453 like to acknowledge and thank the R/V Mário Ruivo for the ship-time and support of the crew. The  
454 authors would like to acknowledge that the research for this study was conducted at the Centre of Marine  
455 Sciences (CCMAR), University of Algarve, Faro, Portugal and the Portuguese Institute for the Sea and  
456 Atmosphere (IPMA, I.P.), Lisboa, Portugal.

#### 457 **References**

- 458 Ambar I., A shallow core of Mediterranean water off western Portugal. *Deep-Sea Res* 30(6A):677-  
459 680, 1983.
- 460 Ambar, I., Serra, N., Neves, F., and Ferreira, T., Observations of the Mediterranean Undercurrent and  
461 eddies in the Gulf of Cadiz during 2001, *J. Mar. Sys.*, 71, 195–220, 2008.

462 Arístegui, J., Álvarez-Salgado, X., Barton, E., Figueiras, F., Hernández-León, S., Roy, C., Santos, A.,  
463 Oceanography and fisheries of the Canary Current/Iberian region of the eastern North Atlantic. In:  
464 Robinson, A., Brink, K. (Eds.), *The Sea, In: The Global Coastal Ocean: Interdisciplinary Regional*  
465 *Studies and Syntheses*, vol. 14 (Part B). Harvard University Press, Cambridge, MS, pp. 877–931,  
466 2006.

467 Bower, A., L. Armi, and I. Ambar, Direct evidence of meddy formation off the southwestern coast of  
468 Portugal. *Deep-Sea Res.*, 42, 1621–1630, 1995.

469 Cardeira S., F. Rita, P. Relvas, A. Cravo, Chlorophyll *a* and chemical signatures during an upwelling  
470 event off the South Portuguese coast (SW Iberia). *Continental Shelf Research* 52, 133–149. 2013.  
471 <http://doi.org/10.1016/j.csr.2012.11.011>

472 Coppola, L., Ntoumas, M., Bozzano, R., Bensi, M., Hartman, S. E., CharcosLlorens, M. I., et al. (2016).  
473 Handbook of Best Practices for Open Ocean Fixed Observatories. European Commission, FixO3  
474 Project, 127. (European Commission, FixO3 project, FP7 Programme 2007-2013 under grant  
475 agreement n° 312463). Available online at: <http://hdl.handle.net/111penalty-\@M329/302>

476 Garel, E.; Laiz, I.; Drago, T.; Relvas, P., Characterisation of coastal counter-currents on the inner shelf  
477 of the Gulf of Cadiz. In: *Journal of Marine Systems* 155, S. 19–34., 2016

478 Hald, A., *Statistical theory with engineering applications*, John Wiley Sons, New York, ISBN-10  
479 0471340561, 1952.

480 IOOS QUARTOD, Manual for Real-Time Quality Control of Dissolved Oxygen Observations,  
481 Version 2.1, August, 2018,  
482 [https://cdn.ioos.noaa.gov/attachments/2018/08/QARTOD\\_DOSecondUpdate\\_final.pdf](https://cdn.ioos.noaa.gov/attachments/2018/08/QARTOD_DOSecondUpdate_final.pdf), (last access:  
483 27 March 2023)

484 Janeiro, J., Neves, A., Martins, F., and Relvas, P., Integrating technologies for oil spill response in the  
485 SW Iberian coast, *Journal of Marine Systems*, Volume 173, 31-42, 2017.

486 Macias, D. M., Guerreiro, C. T., Prieto, L., Peliz, A. and Ruiz, J., A high-resolution hydrodynamic-  
487 biogeochemical coupled model of the Gulf of Cadiz – Alboran Sea region”, *Mediterranean Marine*  
488 *Science*, 15(4), pp. 739–752, 2014.

489 Mauritzen C., Morel Y., Paillet J., On the influence of Mediterranean water on the central waters of  
490 the North Atlantic Ocean , *Deep-Sea Research I*, vol. 48 (pg. 347-38), 2001.

491 McDougall, T. J., & Krzysik, O. A., Spiciness, *Journal of Marine Research*, 73(5), 141–152. 2015.  
492 <https://doi.org/10.1357/002224015816665589>

493 OceanSITES, Data Format Reference Manual, Version 1.4. ,2020.  
494 [http://www.oceansites.org/docs/oceansites\\_data\\_format\\_reference\\_manual.pdf](http://www.oceansites.org/docs/oceansites_data_format_reference_manual.pdf) (last access: 27 March  
495 2023)

496 PABIM (Platforms for Biogeochemical studies: Instrumentation and Measure), White book on oceanic  
497 autonomous platforms for biogeochemical studies: Instrumentation and measure, Version 1.3,  
498 February 2010.  
499 [https://www.coriolis.eu.org/content/download/3150/23513/file/2009\\_PABIM\\_white\\_book\\_version1.3.](https://www.coriolis.eu.org/content/download/3150/23513/file/2009_PABIM_white_book_version1.3.pdf)  
500 [pdf](https://www.coriolis.eu.org/content/download/3150/23513/file/2009_PABIM_white_book_version1.3.pdf), (last access: 27 March 2023)

501 Rautenbach Sarah, Relvas Paulo, Sousa Carlos (2022). EMSO-Iberian Margin Cape St. Vincent  
502 observatory data (subsurface mooring) from Jun-Oct 2022. SEANOE. <https://doi.org/10.17882/94769>

503 Relvas, P., and E.D. Barton, Mesoscale patterns in the Cape São Vicente (Iberian Peninsula) upwelling  
504 region, *Journal of Geophysical Research*, 107(C10), 3164, doi:10.1029/2000JC000456, 2002.

505 Relvas, P., and E. D. Barton, A separated jet and coastal counterflow during upwelling relaxation off  
506 Cape São Vicente (Iberian Peninsula), *Continental Shelf Research*, 25, 29-49, 2005.

507 Sánchez-Leal, R.F., M. J. Bellanco, L. M. Fernández-Salas, J. García-Lafuente, M. Gasser-Rubinat, C.  
508 González-Pola, F. J. Hernández-Molina, J. L. Pelegrí, A. Peliz, P. Relvas, D. Roque, M. Ruiz-  
509 Villarreal, S. Sammartino, J. C. Sánchez-Garrido, The Mediterranean Overflow in the Gulf of Cadiz:  
510 A rugged journey. *Sci. Adv.* 3, eaao0609 (2017) <https://doi.org/10.1126/sciadv.aao0609>

511 SeaDataNet, Data Quality Control Procedures, 6th Framework of EC DG Research, Version 2.0, May  
512 2010, <https://www.seadatanet.org/Standards/Data-Quality-Control> (last access: 27 March 2023)

513 Serra N, Ambar I, Boutov D, Surface expression of Mediterranean Water dipoles and their  
514 contribution to the shelf/slope–open ocean exchange. *Ocean Sci* 6:191–209, 2010.

515 Wilkinson, M. D., Dumontier, M., Appleton, G., Axton, M., Baak, A., Blomberg, N., et al. (2019).  
516 Addendum: the FAIR guiding principles for scientific data management and stewardship. *Sci. Data* 6:6.  
517 doi: 10.1038/s41597-019-0009-6

518